Available online at www.sciencedirect.com
ScienceDirect
Journal of Catalysis 245 (2007) 326–337
JOURNAL OF CATALYSIS
www.elsevier.com/locate/jcat

Steam reforming of ethanol over Pt/ceria with co-fed hydrogen

Gary Jacobs, Robert A. Keogh, Burtron H. Davis *

Center for Applied Energy Research, 2540 Research Park Drive, Lexington, KY 40511, USA

Received 9 March 2006; revised 13 October 2006; accepted 19 October 2006

Available online 28 November 2006

Abstract

Metal/ceria catalysts are receiving great interest for reactions involving steam conversion, including CO for low-temperature water–gas shift, and the conversion of chemical carriers of hydrogen, among them methanol, and ethanol. The mechanism by which ROH model reagents are activated on the surface of the Pt/partially reduced ceria catalyst was explored using a combination of reaction testing and infrared spectroscopy. In this particular investigation, the activation and turnover of ethanol were explored and compared with previous investigations of methanol steam reforming and low-temperature water–gas shift under H_2-rich conditions, where the surface of ceria is in a partially reduced state. Under these conditions, activation of ethanol was found to proceed by dissociative adsorption at reduced defect sites on ceria (i.e., Ce surface atoms in the Ce^{3+} oxidation state), yielding an adsorbed type II ethoxy species and an adsorbed H species, the latter identified to be a type II bridging OH group. In the presence of steam, the ethoxy species rapidly undergoes molecular transformation to an adsorbed acetate intermediate by oxidative dehydrogenation. This is analogous to the conversion of type II methoxy species to formate observed in previous investigations of methanol steam reforming. In addition, although formate then decomposes in steam to CO_2 and H_2 during methanol steam reforming, in an analogous pathway for ethanol steam reforming, the acetate intermediate decomposes in steam to CO_2 and CH_4. Therefore, further H_2 production requires energy-intensive activation of CH_4, which is not required for methanol conversion over Pt/ceria.

Keywords: Cerium oxide; CeO_2; Platinum; Pt; Hydrogen; H_2; Steam reforming; Ethanol; Acetic acid; Methanol; Formate; Methoxy; Methoxide; Ethoxy; Ethoxide; Acetate; Fuel cell; Water–gas shift

1. Introduction

The main drivers that will determine the possibility of a hydrogen-based economy will be the achievement of key breakthroughs, cost reductions at all stages of development, and, certainly, government policies [1]. Infrastructure options for producing and delivering hydrogen currently under consideration include, among other competing technologies (e.g., hydrogen pipelines, cryogenic storage of hydrogen, metal-hydrides), the central production of high-energy density carriers, like methanol and ethanol, transport to a point of use, and reforming to release the hydrogen for fuel cell applications [2]. In terms of fuel flexibility, methanol has a distinct advantage over ethanol in that it can be produced from either CO and H_2 or CO_2 and H_2, syngas sources that can be derived from the steam reforming of hydrocarbons or gasification of coal and biomass. In the future, it is conceivable that methanol also could be produced from atmospheric CO_2 and H_2 generated by electrolysis using nuclear energy, as pointed out by Olah [3]. Ethanol, on the other hand, is receiving interest as a bio-fuel produced from the fermentation of corn and other renewable resources [4–6].

However, from the standpoint of steam-reforming catalysis, as a chemical carrier for hydrogen, methanol may offer other advantages, as highlighted in this work. Probably the two most important catalyst systems for hydrogen production applications include the M/ZnO (M = Cu, Pd) and M/CeO_2 systems, typically promoted by Pt, Pd, or other metals [7,8]. As seen in a review of the literature, these catalysts are used extensively in applications including conventional, oxidative, and autothermal steam reforming of alcohols like methanol (M/ZnO [9–38], M/CeO_2 [39–45]) or ethanol (M/ZnO [46–51], M/CeO_2 [52–57]), water–gas shift, and preferential oxidation of CO. The latter two reactions require a vast citation index, as detailed in some general reviews [7,8].

* Corresponding author.
E-mail address: davis@caer.uky.edu (B.H. Davis).

0021-9517/$ – see front matter
doi:10.1016/j.jcat.2006.10.018

The aims of the current investigation are to gain insight into the mechanism operating for the steam reforming of ethanol reaction over a Pt/ceria catalyst under hydrogen-containing conditions, and also to compare the findings with proposed mechanisms for related reactions, including water–gas shift and methanol steam reforming. That is, it is the goal of this work to assess how ethanol, as a model compound of the type ROH, is activated and turns over on sites consisting of partially reduced ceria in close proximity to Pt metal clusters. The ideal stoichiometry for hydrogen production from alcohol steam reforming is as follows:

Ethanol steam reforming:

$$CH_3CH_2OH + 3H_2O \leftrightarrow 6H_2 + 2CO_2 \quad (\Delta H_{298\,K},\ 1\ \text{bar} = 347.4\ \text{kJ/mol}), \tag{1}$$

Methanol steam reforming:

$$CH_3OH + H_2O \leftrightarrow 3H_2 + CO_2 \quad (\Delta H_{298\,K},\ 1\ \text{bar} = 131\ \text{kJ/mol}). \tag{2}$$

It is also well known that the water–gas shift reaction significantly influences the hydrogen yield,

Water–gas shift:

$$CO + H_2O \leftrightarrow 3H_2 + CO_2 \quad (\Delta H_{298\,K},\ 1\ \text{bar} = -41.2\ \text{kJ/mol}). \tag{3}$$

The method of comparing the reactivity of families of model compounds (e.g., ROH) has been extensively applied in the past. For example, Hutchings et al. [58] used the technique to probe the water–gas shift mechanism over Co and Cu/MnO catalysts. They reported that the key difference between a water–gas shift mechanism involving O adatoms (which may arise from hydroxyl group decomposition) in a regenerative (i.e., redox) process and one involving hydroxyl groups via a formate-type intermediate lies in how the water molecule decomposes on the surface. To probe the process on Cu/MnO, they used model molecules related to the H_2O molecule, including CH_3OH and CH_3CH_2OH. They concluded that methanol dissociates to give a methoxy intermediate and adsorbed H. They observed an analogous mechanism for ethanol dissociation. This result strongly suggests that water dissociates to give OH and H on the surface, and that the water–gas shift mechanism likely proceeds via an associative mechanism.

In 2005, Rioche et al. [59] examined the steam reforming of model compounds in relation to the steam reforming of bio-oil produced from biomass pyrolysis. They reported an important support effect with the addition of ceria–zirconia promoter to the catalyst over alumina alone during the conversion of acetic acid, acetone, ethanol, and phenol. The Pt/ceria–zirconia catalyst exhibited relatively good stability during a 9-h test, but temperatures above 800 °C were needed to achieve high yields of hydrogen and carbon oxides (i.e., CO, CO_2) from ethanol, considerably higher than the reforming temperatures (400–500 °C) required to achieve significant conversion of methanol, which we reported that same year over Pt/ceria [44].

To probe the mechanism by which ethanol is activated and converts over Pt/ceria, we used a combination of in situ DRIFTS spectroscopy and fixed-bed reaction tests. Finally, we contrast the reformability of ethanol with our previous findings for methanol steam reforming from a mechanistic perspective.

2. Experimental

2.1. Catalyst preparation

Ceria with high surface area (∼110 m^2/g) was prepared by homogeneous precipitation of cerium nitrate using urea to slowly release the precipitating agent, the hydroxide anion. The resulting cerium hydroxide material was calcined at 400 °C for 4 h to produce nanoscale crystallites of CeO_2. To load the platinum, ceria was impregnated with an aqueous solution of tetraammine platinum (II) nitrate, and the catalyst was aged overnight at room temperature, dried in a muffle furnace at 110 °C for 8 h, and recalcined at 350 °C for 4 h, to decompose the platinum precursor. Details of the procedure are provided elsewhere [60], and background for the method has been given by Li et al. [61].

2.2. BET surface area

BET surface area measurements on the ceria and Pt/ceria materials were conducted using a Micromeritics Tristar 3000 gas adsorption analyzer. Approximately 250 mg of catalyst was used in each trial. A full 70-point isotherm was obtained at the boiling temperature of N_2 using N_2 as the adsorbate.

2.3. Catalyst activation

Activation of the ceria and Pt/ceria catalysts in hydrogen was followed by (1) temperature-programmed reduction (TPR), (2) X-ray absorption near-edge spectroscopy (XANES), and (3) diffuse reflectance infrared Fourier transform spectroscopy (DRIFTS). Details of these procedures were provided previously [60]; a brief description is given here. TPR was conducted using a Zeton-Altamira AMI-200 unit, equipped with a thermal conductivity detector (TCD). Argon served as the reference gas, and 10% H_2 (balance Ar) was flowed at 30 cm^3/min as the temperature was increased from 50 to 1100 °C. XANES was carried out using a fabricated in situ flow cell at the Ce L_{III} (5723 eV) edge at beamline X18b, Brookhaven National Laboratory, Upton, New York. Smooth self-supporting, pinhole-free pellets were pressed and loaded into the cell, and the treatment gas (H_2) was directed directly at the sample area. Scans were obtained in transmission mode as the cell temperature was raised in 50 °C increments. Partial reduction of ceria was observed to occur at ∼250 °C. Linear combination XANES fits of treated catalysts with reference standards were carried out using WinXAS [62].

2.4. DRIFTS

DRIFTS spectra were obtained using a Nicolet Nexus 870 spectroscope equipped with a DTGS-TEC detector. A high-pressure/high-temperature cell fitted with ZnSe windows (Thermo Spectra-tech) served as the reaction chamber for in situ adsorption and reaction measurements. The gas lines leading to and from the rector were heat-traced to prevent condensation and were also covered with ceramic fiber tape and insulating

wrap. Scans were taken at a resolution of 4 to give a data spacing of 1.928 cm^{-1}. Typically, 128 scans were obtained to improve the signal-to-noise ratio. The sample amount was 33 mg of catalyst.

A vaporizer consisted of a downflow tube packed with quartz beads and quartz wool heated by a ceramic oven, with the temperature was monitored via an internal thermocouple. The steam generator and lines were run at the same temperature as that of the in situ sample holder of the DRIFTS cell. Water was pumped into the system using a precision ISCO model 500D syringe pump through a welded 1.6-mm line. First, the catalyst was slowly ramped and activated in H_2 (100 cm^3/min) for 30 min. During the ramping cycle, scans were taken at 50 °C intervals to monitor the activation step. Ethanol or acetic acid adsorption experiments were carried out by passing inert nitrogen gas (50 cm^3/min) through a bubbler. Then steam (65 cm^3/min), mixed with N_2 (135 cm^3/min), was used to decompose the adsorbed complexes at different temperatures of interest. Snapshots were taken after purging in N_2 (135 cm^3/min) to capture the different species present on the surface during decomposition. Inert nitrogen gas and hydrogen were controlled using Brooks 5850 series E mass flow controllers. The gas lines were filtered using Supelco O_2/moisture traps.

2.5. Testing in a fixed-bed reactor

Steady-state ethanol and acetic acid conversion measurements were conducted using a fixed-bed reactor system consisting of a 0.5-inch-diameter stainless steel tube with an internal thermocouple. Experiments were carried out using 33 mg of catalyst diluted to 0.4 g with silica. The catalyst bed was supported on a bed of quartz glass wool. The vaporizer, gas delivery system, and ancillary equipment were as described in Section 2.4. Water and ethanol or water and acetic acid were fed to the vaporizer during studies, producing gas flow rates of 3.75 and 125 cm^3/min, respectively (1 atm, 20 °C). H_2 (100 cm^3/min) and N_2 (10 cm^3/min) were also included in the feed. The liquid phase was knocked out of the product gas stream using either a solid drying agent or, in the case of liquid phase measurements, a dry ice trap. The gas products were monitored on-line using an SRI gas chromatograph equipped with dual columns, dual analyzers (thermal conductivity and flame ionization detector), and a methanizer, which allows for the conversion of CO and CO_2 products to CH_4 for more accurate analysis. For acetic acid conversion, liquid samples were collected and analysis of the aqueous solution was performed using a HP 5790 gas chromatograph equipped with a TCD. The separation of the compounds of interest was accomplished using a 6 foot × 1/8 inch (80/100 mesh) Porapak Q packed column. Quantitation was performed using a HP 3396 Series 11 integrator. Identification of the compounds was carried out using standards and an Agilent GC/MS.

In one ethanol steam-reforming experiment, CO_2/CO product selectivity was monitored as a function of H_2 concentration. N_2 was used as a balancing gas to maintain constant space velocity, ethanol feed partial pressure, and steam feed partial pressure. During another ethanol steam-reforming experiment, CO_2 product yield was recorded while H_2O was replaced by an equivalent molar amount of D_2O to assess the possibility of a kinetic isotope effect. An analogous experiment was carried out for acetic acid steam reforming.

3. Results

3.1. Characterization of catalyst geometric and electronic properties

The results of nitrogen physisorption measurements are summarized in Table 1. The BET surface area of the resulting calcined ceria material was ∼110 m^2/g, whereas the 1% Pt/ceria catalyst had a surface area of ∼108 m^2/g. A slight increase in the average pore radius after loading the Pt was seen, from 1.45 to about 1.50 nm, normally attributed to blocking of the narrowest pore by the metal clusters.

The resulting profiles from TPR of the unpromoted and Pt promoted ceria catalysts are shown in Fig. 1. Two distinct features characterize the reduction processes that occur with ceria catalysts: a surface shell reduction step and a bulk reduction step. For unpromoted ceria, the surface shell reduction step occurs over the range of 400–550 °C, whereas the bulk reduces above 750 °C. For 1% Pt/ceria, although the bulk is little affected by the presence of the metal promoter, the surface shell reduction step is facilitated to the 250–300 °C range. We previously observed by XANES spectroscopy [60] that the metal promoter reduces at a temperature slightly lower than that of the ceria surface shell reduction, suggesting that the metallic phase of Pt is important for the promoting effect on ceria. The partial

Table 1
Results of BET surface area and porosity measurements

Catalyst	BET SA (m^2/g)	Average pore volume (cm^3/g)	Average pore radius (nm)
Ceria	109.8	0.797	1.45
1% Pt/ceria	108.3	0.0806	1.49

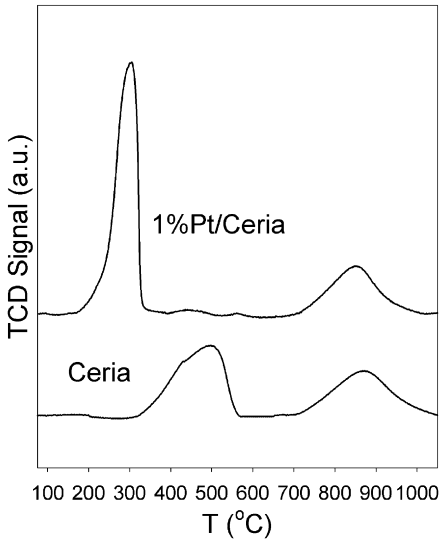

Fig. 1. H_2 TPR profiles for unpromoted ceria and 1% Pt/ceria catalysts.

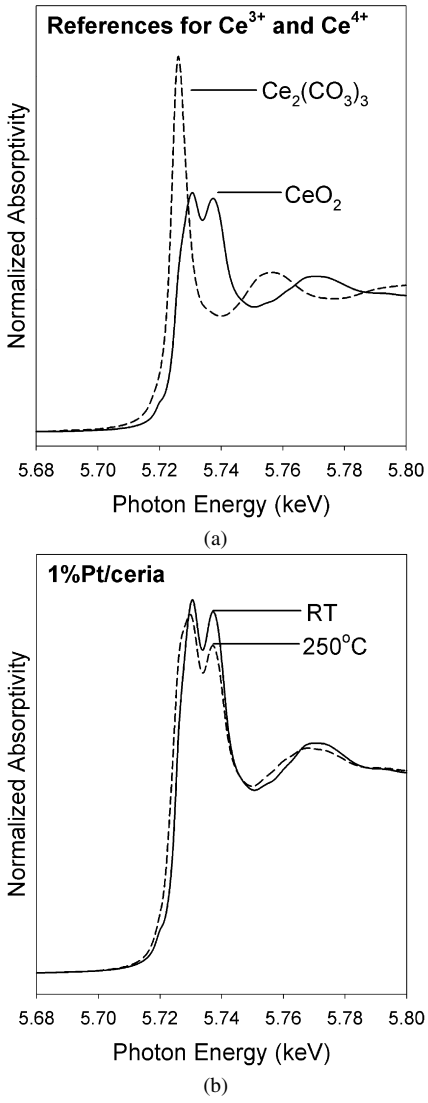

Fig. 2. XANES spectra at the Ce L_{III} edge for (a) reference compounds for the Ce^{3+} and Ce^{4+} oxidation state and (b) the 1% Pt/ceria catalyst before and after surface shell reduction, which takes place at ∼250 °C. The extent of reduction was ∼20%.

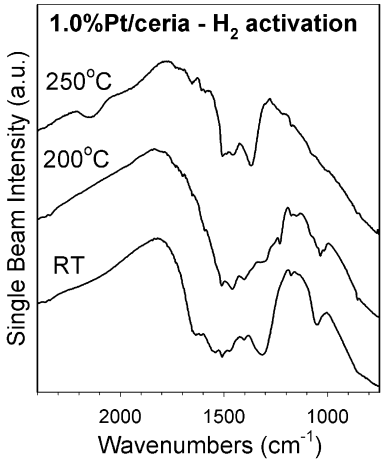

Fig. 3. Single beam intensity DRIFTS spectra for the reduction of Pt/ceria in hydrogen. A remarkable decrease in intensity of OCO stretching bands for carbonate species is observed after the surface activation step.

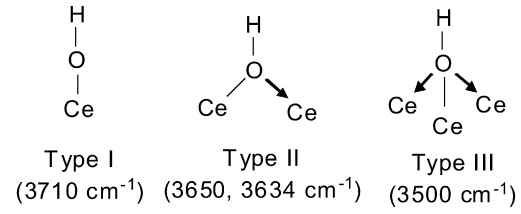

Scheme 1. OH groups as a function of degree of coordinative unsaturation.

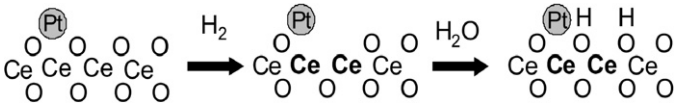

Scheme 2. Activation of ceria surface via vacancy formation.

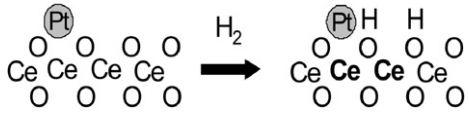

Scheme 3. Activation of ceria surface via hydrogen dissociation and spillover.

reduction of ceria is confirmed by XANES spectroscopy measurements (Fig. 2b) where, after reduction at 250 °C in flowing hydrogen, the XANES profile changes shape to resemble a combination of the two oxidation states. Reference spectra are provided in Fig. 2a. Taking a linear combination of the two reference spectra using WinXAS [62], the extent of reduction is estimated to be about 20% at 250 °C. This value is close to that reported previously [63], indicating complete reduction of the monolayer. Often neglected in considering the reduction of surface ceria, DRIFTS spectra, displayed in Fig. 3, indicate that a considerable fraction of surface carbonate species, always present on basic oxides, decompose at the precise temperature at which the reduction step occurs. We have previously shown [60] that type II bridging OH groups (∼3650 cm^{-1}) are activated on the surface of partially reduced ceria, once reduction has taken place. The type II bridging OH groups were identified in a detailed spectroscopic investigation by Laachir et al. [63] of how the degree of reduction of the surface shell of ceria impacts the degree of coordination of the surface OH groups with the Ce atoms, as shown in Scheme 1.

In our previously reported water–gas shift studies over Pt/ceria [60], we identified two pathways for the formation of the type II bridging OH groups over Pt/partially reduced ceria. They are either formed by reduction of the ceria surface from Ce^{4+} to Ce^{3+}, followed by the dissociative adsorption of H_2O at the defects (Scheme 2), or directly, via the dissociation of H_2 on Pt and subsequent spillover of atomic hydrogen to the ceria surface, reducing the cerium atoms associated with OH groups from Ce^{4+} to Ce^{3+} (Scheme 3). Support for the latter view comes from earlier XANES tests, which indicated that Pt reduced at a temperature slightly lower than that observed for the partial reduction of ceria.

Note that in each of the above schemes, the surface shell Ce atoms in bold type are in the Ce^{3+} oxidation state.

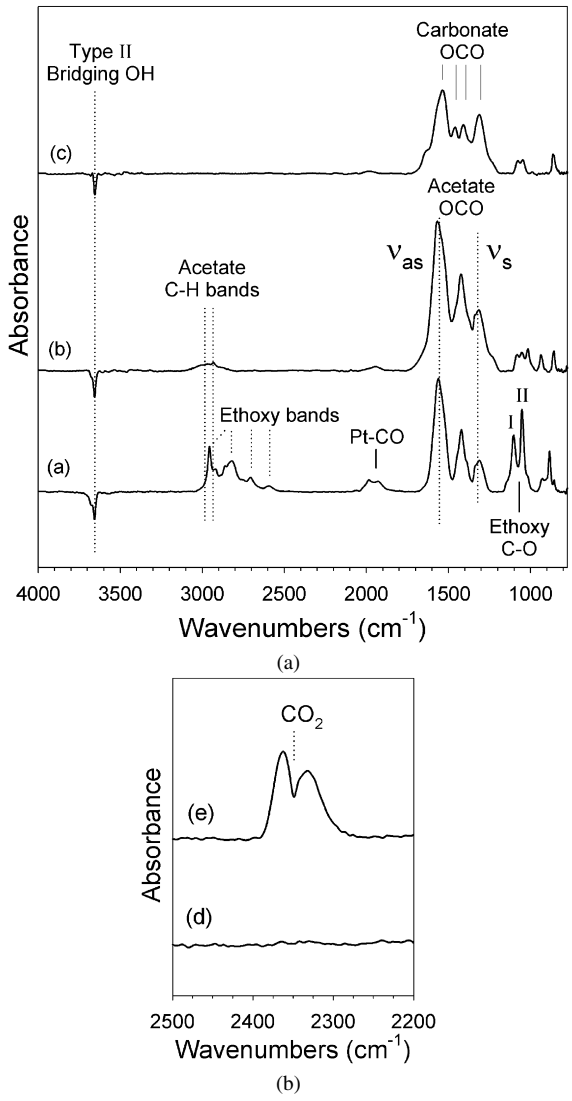

Fig. 4. DRIFTS spectra for, moving upward, (a) adsorption of ethanol at 160 °C, (b) after steaming the catalyst at 160 °C for ∼20 min and purging with N_2 and (c) after steaming the catalyst at 250 °C for ∼20 min and purging with N_2. During steaming of the ethoxy species, (d) little CO_2 was generated. However, (e) CO_2 was generated once carbonate was formed from the decomposition of the acetate intermediate.

3.2. *In situ DRIFTS spectroscopy*

Based on the preliminary characterization experiments, we conclude that the activated surface involves Pt metal particles situated on a ceria surface that is covered by type II bridging OH groups at the Ce^{3+} cations (i.e., a defect-laden surface). To this surface, different molecules of interest were adsorbed, and the vibrational bands of the molecular species were monitored by DRIFTS.

For DRIFTS experiments, the 1% Pt/ceria catalyst was activated at 300 °C, followed by a nitrogen purge, and cooling to 160 °C before adsorption. As shown in Fig. 4, ethanol was first adsorbed on the surface. It is evident that ethanol adsorbs in a manner which displaces the type II bridging OH groups, because there is a sharp decrease in their band intensity at ∼3650 cm^{-1}. Distinguishing bands for adsorbed ethoxy and,

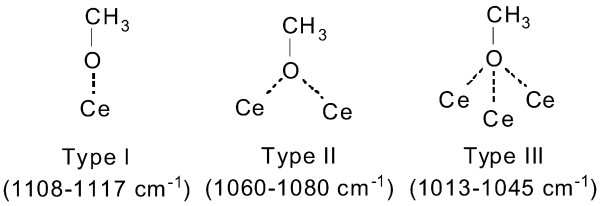

Scheme 4. Methoxy species as a function of coordinative unsaturation.

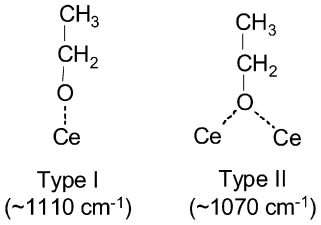

Scheme 5. Proposed ethoxy species as a function of coordinative unsaturation.

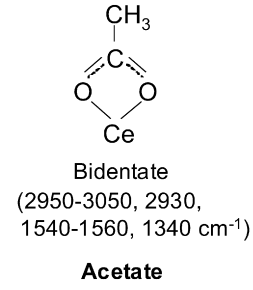

Scheme 6. Infrared band assignments for bidentate acetate.

to a lesser degree, acetate species prevail, along with bands in the range of 1950–2050 cm^{-1} for Pt–CO. Li et al. [64] and Binet et al. [65] have carefully studied the impact of the reduction step on the band positions of adsorbed methanol species over ceria. For example, Binet et al. [65] have shown that the band position for the OC vibration of methoxy species, generated from the adsorption of methanol, is impacted measurably after activation. For the oxidized surface, the OC band appears at ∼1110 cm^{-1} and has been designated type I, whereas the most prevalent band after surface reduction is found in the range of 1060–1080 cm^{-1} and appears to involve complex contributions that give it an asymmetric appearance, as shown in Scheme 4.

In previous work on methanol adsorption to Pt/ceria, [44] we confirmed the appearance of these low wavenumber bands, designated type II methoxy species by Binet et al. [65], and found that with the addition of 1% Pt, the type II methoxy species form at much lower temperatures (∼250 °C vs >450 °C for unpromoted ceria). This is due to the ability of Pt to promote the low-temperature surface reduction of ceria, such that there is higher degree of coordination with the ceria atoms of the oxide component.

With ethanol adsorption, the two analogous bands depicted in Scheme 5 are formed in the range of 1050 to 1120 cm^{-1}, and the band with the greatest intensity is the low-wavenumber one positioned at ∼1070 cm^{-1}, as shown in Fig. 4a.

The bands in the range of 1300–1570 cm^{-1} are due to acetate formation (Scheme 6). Adsorption of acetic acid (Fig. 5, spectrum a) confirms this assignment, because bands with

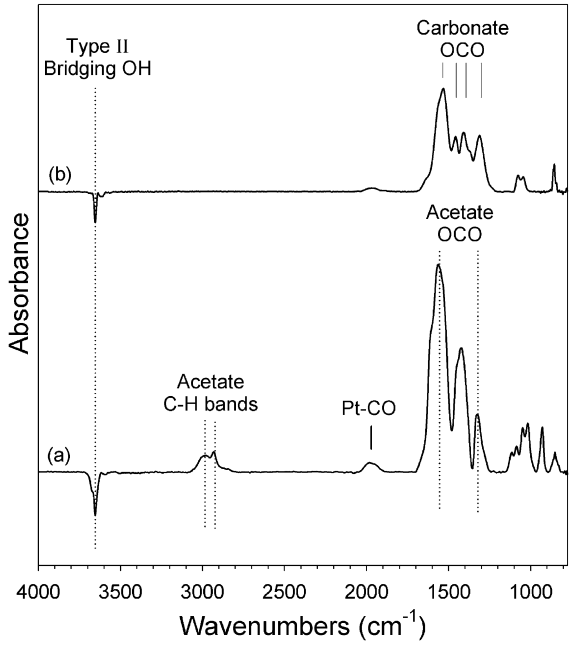

Fig. 5. DRIFTS spectra for, moving upward, (a) adsorption of acetic acid at 160 °C and purging with N_2, (b) after steaming the catalyst at 250 °C for ∼20 min and purging with N_2.

identical position are formed. The most important bands are those in the range of 1540–1560 cm^{-1} assigned to asymmetric OCO stretching and ∼1340 cm^{-1} assigned to symmetric OCO stretching. Accompanying the OCO stretching bands are C–H stretching bands resulting in a broad major band at 2950–3050 cm^{-1}, a sharp band at 2930 cm^{-1}, and minor bands at ∼2850 and 2875 cm^{-1}.

Steaming of the catalyst after adsorption of ethanol at 160 °C, followed by purging in N_2, resulted in a decrease in bands assigned to ethoxy species, and an important increase in those assigned to acetate (Fig. 4, spectrum b). Notice that the shape of the complex series of bands assigned to C–H stretching (2700–3100 cm^{-1}) changes to favor higher-wavenumber bands that resemble precisely those produced from adsorption of acetic acid (compare Fig. 4, spectrum b with Fig. 5, spectrum a). The snapshot that captures the acetate species at this point (Fig. 4, spectrum b) does not reveal any marked change in band intensity for the type II bridging OH groups. Also, as shown in Fig. 4 spectrum d, during steaming, the transformation from ethoxy species to acetate species did not involve any evolution of gas-phase CO_2. However, once the acetate species reached a maximum intensity, further steaming at 250 °C did result in CO_2 production (Fig. 4, spectrum e). At the time of initial CO_2 evolution, the steaming was again arrested, and the catalyst purged in nitrogen. At this point, the acetate bands have disappeared, and it is clear that surface carbonate species have been produced (Fig. 4, spectrum c). The most important bands are located at ∼1290, 1345–1350, 1460, 1500, and 1565 cm^{-1}, indicative of the asymmetric and symmetric OCO stretching vibrations of unidentate, bidentate, and polydentate carbonates, in good agreement with the well-documented assignments of, for example, Binet et al. [65] (provided in Scheme 7) and Holmgren et al. [66]. It is noteworthy to point out that, according to the band intensity at 3650 cm^{-1}, a fraction of the type II bridging OH groups were replenished during CO_2 evolution. Fig. 5, spectrum b shows that steaming of the adsorbed acetate species produced from acetic acid adsorption also led to the conversion of adsorbed acetate to carbonate species.

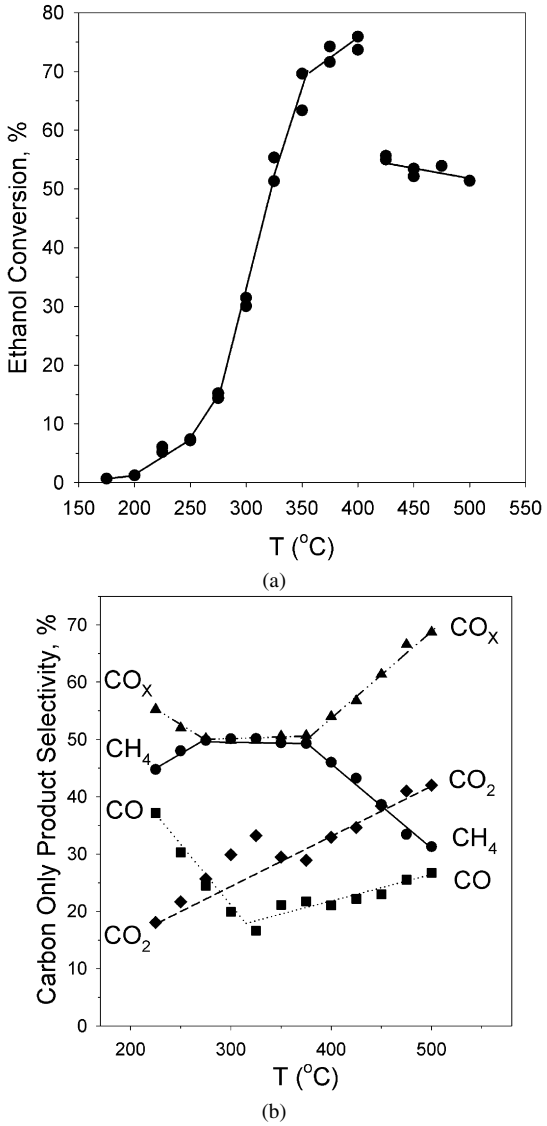

Fig. 6. Fixed bed reactor testing data for the steam reforming of ethanol, including (a) conversion and (b) gas phase product selectivity versus temperature. Methane selectivity was observed to be precisely 50% between the range 250 to 400 °C.

3.3. Fixed-bed reaction testing

Results of fixed-bed reaction testing in the range of 175 to 500 °C are reported in Figs. 6a–6b, and the major carbon-containing products detected were methane, carbon dioxide, and carbon monoxide, whereas hydrogen production was calculated from the carbon product distribution. In Fig. 6a, the ethanol conversion is

$$X(\mathrm{EtOH}) = (\mathrm{CH_3CH_2OH\ in} - \mathrm{CH_3CH_2OH\ out}) / \mathrm{CH_3CH_2OH\ in}.$$

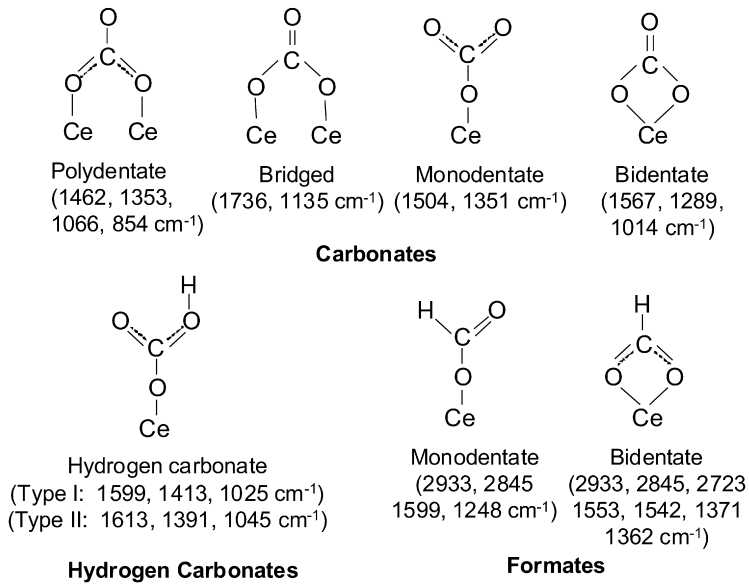

Scheme 7. Infrared band assignments for formate and carbonate species.

Table 2
Response of CO_2/Co ratio to H_2 concentration during ethanol steam reforming

Condition	N_2 (ccm)	H_2 (ccm)	CO Sel	CO_2 Sel	CH_4 Sel	CO_2/CO	X_{EtOH}
1	0	100	31.8	18.8	49.4	0.59	34.4
2	25	75	30.6	21.0	48.4	0.69	30.7
3	50	50	28.9	23.2	47.9	0.80	35.6
4	75	25	26.2	25.6	48.3	0.98	30.9
5	100	0	19.9	52.1	28.0	2.74	5.4
6	75	25	24.9	37.8	37.2	1.52	9.9

Note. CH_3CH_2OH gas flow: 3.75 ccm; H_2O gas flow: 125 ccm; T: 300 °C; 33 mg 1% Pt/ceria catalyst.

Two different selectivities are typically reported for ethanol steam reforming, total molar product selectivity, and/or carbon product selectivity (Fig. 6b). We chose the latter, which is based on measured values. Total molar product selectivity is defined to be the moles of one product divided by the total moles of product, whereas carbon product selectivity is the selectivity of a carbon-containing product divided by the total moles of carbon-containing products, as follows:

Total molar product selectivity:

$$S(CO_2) = CO_2 / (CO_2 + CO + CH_4 + H_2),$$

Carbon product selectivity:

$$S(CO_2) = CO_2 / (CO_2 + CO + CH_4).$$

Regarding the mechanism of ethanol steam reforming, in the temperature range of 225–400 °C, the most telling finding comes from the carbon product selectivity, which consisted of approximately 50% methane, with CO and CO_2 making up the additional 50%. These results imply that CO_2 and methane are primary products and that CO is produced as a secondary product from the reverse water–gas shift reaction:

$$CH_3CH_2OH + H_2O \leftrightarrow CH_4 + CO_2 + 2H_2, \quad (4)$$

$$CO_2 + H_2 \leftrightarrow CO + H_2O. \quad (5)$$

The implication, then is that to achieve further increases in H_2 production, the CH_4 must be further reformed, which is an energy-intensive process,

$$CH_4 + 2H_2O \leftrightarrow 4H_2 + CO_2 \quad (\Delta H_{298\,K},\ 1\ \text{bar} = 253\ \text{kJ/mol}). \quad (6)$$

The findings therefore allow us to estimate the moles of H_2 produced. Until the CH_4 carbon product selectivity drops below 50%, the moles of H_2 produced will be strictly from reaction (4), minus that which is converted by reverse water–gas shift, such that the number of moles of H_2 produced follow the expression $2 \times (\text{moles } CO_X) - \text{moles CO}$. When the CH_4 carbon product selectivity does drop below 50% at higher temperatures (i.e., >400 °C), the additional number of moles of H_2 produced will follow $4 \times (0.5 - \text{moles } CH_4 \text{ reacted})$ from reaction (6) minus the additional moles of CO produced from reaction (5).

To probe the conclusion that CH_4 is one of the main primary products, and relatively unreactive at and below 400 °C, the sensitivity of the CO_2/CO ratio response to changes in hydrogen partial pressure was recorded. As shown in Table 2, decreasing the H_2 content from 100 to 25 ccm (while maintaining constant space velocity, ethanol, and steam partial pressures using N_2-balancing gas) did not change the conversion, but rather led to systematic increases in the CO_2/CO ratio, signifying that the turnover rate of ethanol is not affected, but only the CO_2/CO

Table 3
Results of isotope switching in fixed bed catalytic testing

$T = 300\,^{\circ}C$	$H_2O + H_2 + CH_3CH_2OH$			$D_2O + H_2 + N_2 + CH_3CH_2OH$			$H_2O + H_2 + N_2 + CH_3CH_2OH$			KIE
	X_{EtOH}	CO_2 Sel	CO_2 Yd	X_{EtOH}	CO_2 Sel	CO_2 Yd	X_{EtOH}	CO_2 Sel	CO_2 Yd	
Ethanol steam reforming	28.0	22.2	6.2	24.2	16.6	4.0	27.7	22.4	6.2	~1.5
$T = 250\,^{\circ}C$	$H_2O + H_2 + CH_3COOH$			$D_2O + H_2 + N_2 + CH_3COOH$			$H_2O + H_2 + N_2 + CH_3COOH$			KIE
	X_{EtOH}	CO_2 Sel (gas phase products)		X_{EtOH}	CO_2 Sel (gas phase products)		X_{EtOH}	CO_2 Sel (gas phase products)		
Acetic acid reforming	32.9	94.3		31.8	95.3		29.4	94.9		~1.0

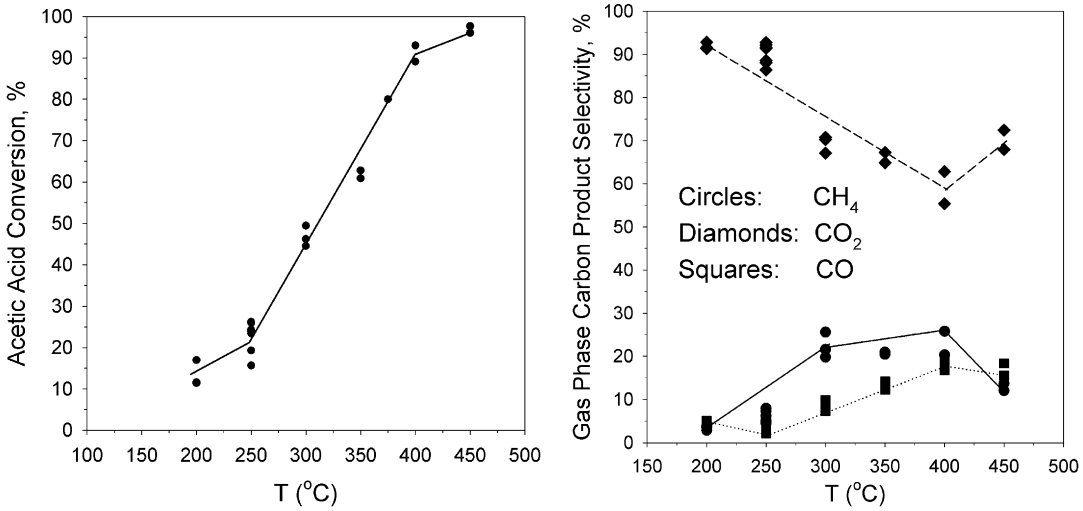

Fig. 7. Fixed bed reactor testing data for the steam reforming of acetic acid, including (a) conversion and (b) gas phase carbon product selectivity versus temperature. The high carbon dioxide selectivity is indicative of acetic acid ketonization, whereby acetone was trapped in the liquid product phase.

product selectivity increases, presumably due to a lower reverse water–gas shift rate. When co-fed H_2 was absent from the feed, the catalyst quickly deactivated, perhaps by surface reoxidation. When 25 cm of H_2 was returned to the feed (Table 2), some reactivation of the catalyst was observed, although the catalyst did not quickly regain its original activity.

Isotope switching from H_2O to D_2O was carried out to further shed light on the mechanism of ethanol steam reforming over Pt/ceria. As shown in Table 3, switching from H_2O to D_2O led to a decrease in both ethanol conversion and CO_2 product selectivity, resulting in a remarkably lower relative CO_2 product yield. The resulting normal kinetic isotope effect was ~1.5.

The role of adsorbed acetate during the ethanol turnover observed in DRIFTS led us to explore acetic acid conversion. Results of fixed-bed reactor testing are summarized in Fig. 7, with acetic acid conversion provided in Fig. 7a and the gas-phase (only) carbon product selectivities given in Fig. 7b. Although the components in the gas-phase products are the same as observed for ethanol steam reforming, the magnitudes of carbon containing gas-phase (only) product selectivities are completely different. Interestingly, carbon dioxide was observed to exhibit the highest gas-phase carbon product selectivity, whereas methane and carbon monoxide were much lower. Clearly, we cannot presume that high CO_2 levels are the result of low-temperature acetic acid steam reforming to hydrogen product. After analysis of six samples of the liquid-phase product, obtained from reaction testing between 350 and 375 °C we observed a high fraction of acetone in the carbon-containing product.

At 250 °C, we carried out isotope switching from H_2O to D_2O, and results are recorded in Table 3. As shown, there was no detectable kinetic isotope effect during steam reforming of acetic acid in switching to the heavier isotope, confirming that acetic acid steam reforming proceeds via a different mechanism than ethanol steam reforming.

4. Discussion

The results paint a compelling picture as to the likely mechanism involved during the steam reforming of ethanol. As CH_4 is produced in an equivalent molar ratio to the total CO_X product produced, it is suggested that ethanol is first converted to CH_4 and CO_2, with CO_2 further reacting in series via reverse water–gas shift, producing CO as a secondary product. The conversion of ethanol to methane effectively produces 2 moles of hydrogen per 1 mole of ethanol. Yet, reverse water–gas shift limits the amount of H_2 produced. Until 400 °C, the maximum

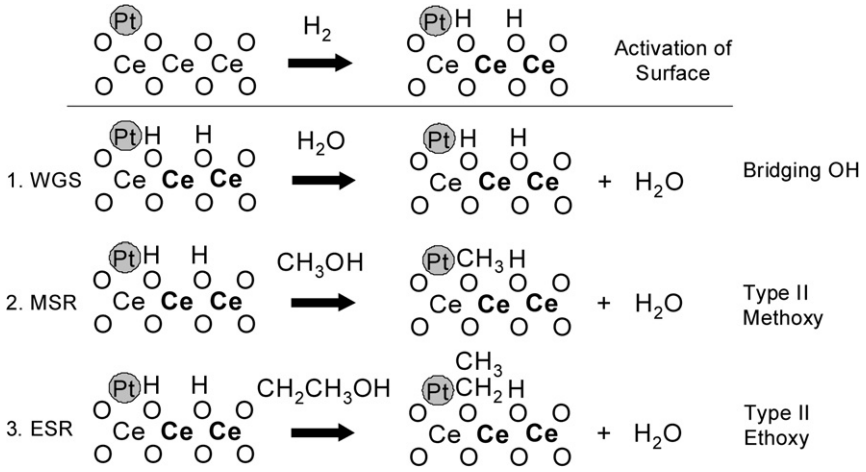

Scheme 8. Activation of the homologous series ROH over Pt/ceria.

amount of hydrogen produced is limited by the inability to activate CH_4

$$CH_3CH_2OH + H_2O \leftrightarrow CH_4 + CO_2 + 2H_2, \quad (4)$$

$$CO_2 + H_2 \leftrightarrow CO + H_2O. \quad (5)$$

Therefore, to achieve further increases in H_2 production, the CH_4 must be steam reformed further, and again the reverse water–gas shift reaction in series will limit the total amount of hydrogen produced,

$$CH_4 + 2H_2O \leftrightarrow 4H_2 + CO_2 \quad (\Delta H_{298\,K},\ 1\ \text{bar} = 253\ \text{kJ/mol}), \quad (6)$$

$$CO_2 + H_2 \leftrightarrow CO + H_2O. \quad (5)$$

Yet, to understand the manner in which ethanol interacts with the surface and turns over to generate CH_4, we resort to the DRIFTS results in comparison with our previous findings for methanol steam reforming. Stepping through the proposed mechanism, it is suggested from the DRIFTS spectra that ethanol adsorbs via dissociative adsorption on the partially reduced ceria to generate a type II ethoxy intermediate and adsorbed H (i.e., as a type II bridging OH group), in the process displacing chemisorbed H_2O by decomposition of the type II bridging OH groups associated with the defect site. This is analogous to what we previously observed during the activation of methanol over Pt/ceria [44], and as previously reported by Binet et al. [65] for adsorption of methanol over partially reduced ceria. It is also analogous to the adsorption of H_2O at defect sites to form the type II bridging OH groups, as reported by Laachir et al. [63] over partially reduced ceria, and as reported by others during water–gas shift over metal/ceria catalysts, including Shido and Iwasawa for Rh/ceria [67] and our own group for Pt/ceria [60]. Therefore, the activation of the homologous series of ROH over Pt/partially reduced ceria is summarized in Scheme 8 as occurring by dissociation at defect sites in the oxide to produce type II adsorbed RO species and adsorbed H.

By DRIFTS, we observe that the reaction of steam with the adsorbed type II ethoxy species results in oxidative dehydrogenation of the ethoxy species to produce adsorbed acetate, the second proposed intermediate involved in the catalysis, resulting in the production of two H_2 molecules by

$$H_2O + CH_3CH_2O^- \Leftrightarrow CH_3COO^- + 2H_2. \quad (7)$$

The analog of this reaction was also observed in our methanol steam reforming investigation, whereby the reaction of steam with methoxy species generated adsorbed formate, by

$$H_2O + CH_3O^- \Leftrightarrow HCOO^- + 2H_2. \quad (8)$$

It has also been proposed [60,67] that, in the water–gas shift reaction, the activated H_2O in the form of bridging OH groups, reacts with CO to produce a formate intermediate, via

$$CO + HO^- \Leftrightarrow HCOO^-. \quad (9)$$

Therefore, the formation of $RCOO^-$ species (i.e., formate, acetate) is proposed to be a common intermediate among the steam reforming of methanol, ethanol, and water–gas shift reactions, as summarized in Scheme 9.

The pathway from adsorbed ethoxide to acetate has not been defined by the current study. A possible pathway is the dehydrogenation of the ethoxy group to adsorbed acetaldehyde followed by the of the aldehyde reaction with OH^- together with the elimination of H_2 together with the formation of the adsorbed acetate. A similar mechanism could apply for methanol, where the step between adsorbed methoxy to formic acid could be an adsorbed formaldehyde. However, data are lacking to support this reaction. The IR data do not show strong peaks for either adsorbed formaldehyde for the conversion of methanol nor acetaldehyde from the conversion of ethanol. The conversion of the acetate when the concentration of acetic acid is high, as when acetic acid is the reactant, leads to the formation of acetone. The reaction of two acid molecules to produce a symmetrical ketone is a well-known reaction in organic chemistry. Likewise, the aldol condensation reaction of an aldehyde is also a well-known organic reaction and in the case of acetaldehyde would result in the formation of a C_4 compound (either 3-hydroxybutaldehyde or 2-butanol (crotonaldehyde)). When acetic acid was used as the charge, significant amounts of acetone were obtained but we did not identify significant amounts of adsorbed acetaldehyde by IR or the dimer 2-butanol

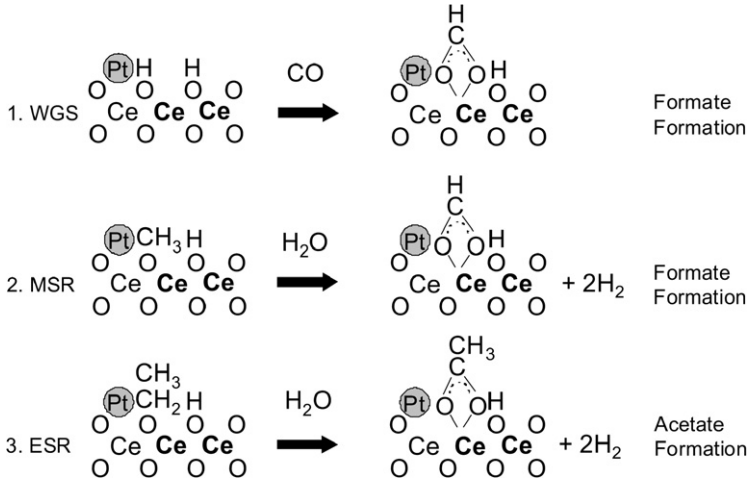

Scheme 9. Formation of the common intermediate $RCOO^-$.

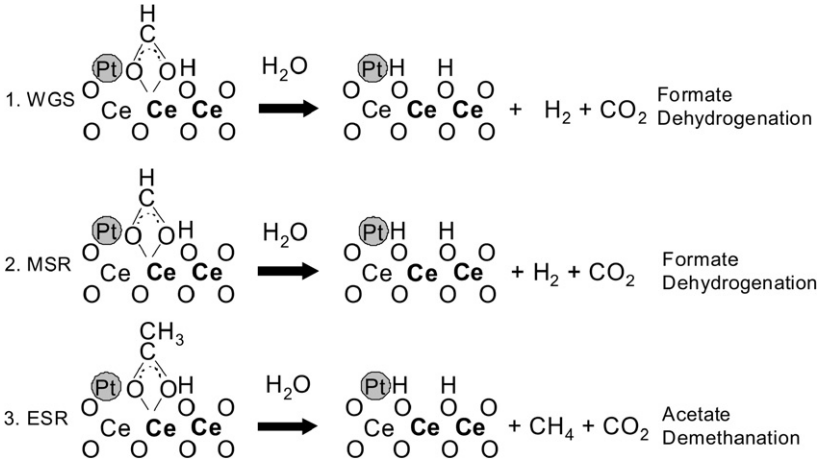

Scheme 10. Acetate demethanation in ESR is the analog of formate dehydrogenation in MSR and WGS.

by GC analysis of the gas phase. It seems reasonable that aldehyde is an intermediate between the alcohol reactant and the acetate intermediate; however, we lack data to verify that this is the case.

Finally, in the presence of steam, the decomposition of the acetate species during ethanol conversion favors demethanation, which is likely assisted by the Pt metal. The carbon dioxide product produced is likely formed from short-lived carbonate species, as suggested by the in situ DRIFTS measurements. In methanol steam reforming, the analog of this step was also observed; however, formate decomposes via dehydrogenation to yield surface carbonate species that further decompose to CO_2. In the water–gas shift, the analog of this is essentially identical, with the formate intermediate decomposing to H_2 and unidentate carbonate, which quickly decomposes to CO_2. Most recently, it has been suggested that a mechanism not unlike that proposed by Grenoble et al. [68–70] is functioning, with formate decomposition being assisted by metal-catalyzed hydrogen abstraction. The three reactions are given in Scheme 10.

Based on the results of reaction testing and DRIFTS, it is strongly suggested that a key feature during the conversion of ethanol over Pt/ceria is the selectivity of the acetate intermediate decomposition, which favors demethanation, as shown in Scheme 11.

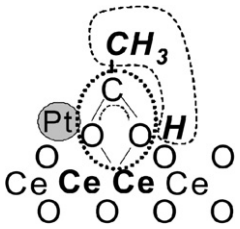

Scheme 11. Demethanation likely occurs at metal–ceria interface.

The steps outlined above yield the following proposed mechanism, Scheme 12, for the catalysis of methane formation as a major reaction occurring during ethanol steam reforming.

The formation of methane may be the rate-determining step of this cycle. The isotope-switching experiment, whereby a KIE of ∼1.5 was observed, certainly suggests that a hydrogen-transfer step is the elementary step that limits the surface catalysis of the demethanation step.

Although the conversion of acetate to methane and carbon dioxide appears to be the primary mechanism of methane formation during ethanol steam reforming, it is interesting that

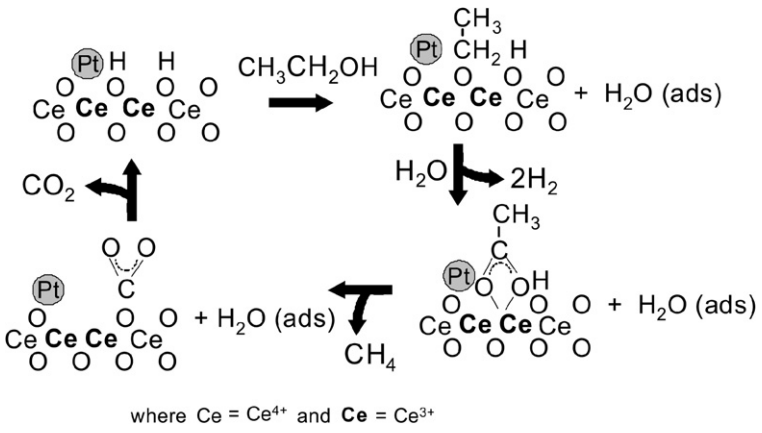

Scheme 12. Proposed ethanol turnover mechanism at low temperature.

acetic acid steam reforming proceeds predominantly via an alternate route. Although methane is produced in small amounts, the major products evolved appear to be acetone and carbon dioxide through ketonization. Here it would seem that coverage effects must come into play. The formation of acetone probably proceeds from the migration of the methyl group from another adsorbed acetate molecule, liberating CO_2 in the process. Again, the DRIFTS results suggest that surface carbonates are involved as the precursor to CO_2 production. Although the probability of such an event occurring would be high in the case of acetic acid conversion, during ethanol steam reforming, the coverage of ethanol is such that it inhibits the probability of two acetic acid molecules being in close proximity, thereby shutting down that mechanism as a significant component. The fact that no measurable kinetic isotope effect is observed during switching from H_2O to D_2O during acetic acid conversion would be in line with a mechanism that excludes hydrogen-transfer steps.

In considering the ethanol steam-reforming results, the data suggest that hydrogen production from ethanol over the Pt/ceria catalysts and conditions used in this work essentially boils down to a problem of methane activation. Although Pt/ceria does activate alcohols by dissociation of the H from the OH group, the problem of methyl group hydrogenation to methane is significant. Because the analog of methane in methanol steam reforming is hydrogen, it would appear that if Pt/ceria catalysts are used in the current context, methanol is better suited to play the role of chemical carrier relative to ethanol, which inevitably requires much higher temperatures to activate, or essentially gasification-type processing (e.g., oxidative steam reforming). In general, it is not surprising that, considering the current literature, Ni and Ni-promoted catalysts are most predominant in the case of ethanol steam reforming [71–80]. Arguably, as suggested by the current study, this is due to the capability of nickel to activate methane or, at the very least, its surface precursor.

5. Conclusion

The results of in situ FTIR and reaction tests indicate that activation of ethanol over partially reduced ceria follows an analogous route as to what has been observed previously for methanol. Ethanol dissociates on the surface to generate type II bridging ethoxy intermediates. In the presence of H_2O, the ethoxy species are converted to adsorbed acetate intermediates via oxidative dehydrogenation, again similar to the transformation of methoxy species to formates during steam reforming of methanol. However, although formates decompose to carbonate species, the precursor to H_2 and CO_2 during methanol steam reforming, the analog for ethanol steam reforming is that acetate is hydrogenated to yield CH_4 and CO_2, indicating that energy-intensive measures are required to achieve further hydrogen production in the case of ethanol processing. Because Pt/ceria catalysts are excellent low-temperature shift catalysts, a reverse water–gas shift occurs in series with ethanol steam reforming to significantly convert the CO_2 and H_2 back to H_2O and CO. When Pt/ceria catalysts are used in the current context to carry out steam-reforming catalysis, the results suggest that methanol may be better suited to the role of chemical carrier for hydrogen.

Acknowledgments

The work was supported by the Commonwealth of Kentucky through a grant from the Kentucky Office of Energy Policy. The authors thank Dr. Syed Khalid for assisting with experiments at the National Synchrotron Light Source (NSLS) at Brookhaven National Laboratory (BNL). Research carried out (in part) at the NSLS at BNL was supported by the US Department of Energy, Division of Materials Science and Division of Chemical Sciences, under contract DE-AC02-98CH10886. The authors also thank Joel Young for fabricating the in situ XAS cell.

References

[1] D. Gielen, G. Simbolotti, Prospects for Hydrogen and Fuel Cells, Organ. for Econ. Coop. and Dev. and the Int. Energy Agency (Claude Mandil, Exec. Dir.), Paris, France, 2005.
[2] U.S. Dept. of Energy, Hydrogen, Fuel Cells, and Infrastructure Technologies Program Multi-year Research, Development, and Demonstration Plan, June, 2003.
[3] G. Olah, Catal. Lett. 93 (2004) 1.
[4] S. Spatari, Y. Zhang, H.L. MacLean, Environ. Sci. Technol. 39 (2005) 9750.
[5] A.E. Farrell, R.J. Plevin, B.T. Turner, A.D. Jones, M. O'Hare, D.M. Kammen, Science 311 (2006) 506.

[6] D. Pimentel, T.W. Patzek, Nat. Res. Res. 14 (2005) 65.
[7] A.F. Ghenciu, Curr. Opin. Solid State Math. Sci. 6 (2002) 389.
[8] R. Farrauto, S. Hwang, L. Shore, W. Ruettinger, J. Lampert, T. Giroux, Y. Liu, O. Ilinich, Annu. Rev. Mater. Res. 33 (2003) 1.
[9] C.J. Jiang, D.L. Trimm, M.S. Wainwright, N.W. Cant, Appl. Catal. A Gen. 97 (1993) 145.
[10] N. Iwasa, S. Kudo, H. Takahashi, S. Masuda, N. Takezawa, Catal. Lett. 19 (1993) 211.
[11] J.C. Amphlett, K.A.M. Creber, J.M. Davis, R.F. Mann, B.A. Peppley, D.M. Stokes, Int. J. Hydrogen Energy 19 (1994) 131.
[12] K. Miyao, H. Onodera, N. Takezawa, React. Kinet. Catal. Lett. 53 (1994) 379.
[13] D. Wang, L. Ma, C.J. Jiang, D.L. Trimm, M.S. Wainwright, D.H. Kim, Stud. Surf. Sci. Catal. 101 (1996) 1379.
[14] G.-C. Shen, S.-I. Fujita, S. Matsumoto, N. Takezawa, J. Mol. Catal. A Chem. 124 (1997) 123.
[15] N. Iwasa, T. Mayanagi, N. Ogawa, K. Sakata, N. Takezawa, Catal. Lett. 54 (1998) 119.
[16] B.A. Peppley, J.C. Amphlett, L.M. Kearns, R.F. Mann, Appl. Catal. A Gen. 179 (1999) 21.
[17] S.P. Asprey, B.W. Wojciechowski, B.A. Peppley, Appl. Catal. A Gen. 179 (1999) 51.
[18] J.P. Breen, J.R.H. Ross, Catal. Today 51 (1999) 521.
[19] L. Ma, D.L. Trimm, M.S. Wainwright, Top. Catal. 8 (1999) 271.
[20] A.W. Grant, J.H. Larsen, C.A. Perez, S. Lehto, M. Schmal, C.T. Campbell, J. Phys. Chem. B 105 (2001) 9273.
[21] J. Agrell, H. Birgersson, M. Boutonnet, J. Power Sources 106 (2002) 249.
[22] M. Saito, J. Wu, K. Tomoda, I. Takahara, K. Murata, Catal. Lett. 83 (2002) 1.
[23] T. Takeguchi, Y. Kani, M. Inoue, K. Eguchi, Catal. Lett. 83 (2002) 49.
[24] V. Subramani, K. Suzuki, C.S. Gopinath, J. Phys. Chem. B 106 (2002) 12737.
[25] Y.-H. Chin, R. Dagle, J. Hu, A.C. Dohnalkova, Y. Wang, Catal. Today 77 (2002) 79.
[26] A.Y. Rozovskii, G.I. Lin, Top. Catal. 22 (2003) 137.
[27] Y. Liu, T. Hayakawa, T. Tsunoda, K. Suzuki, S. Hamakawa, K. Murata, R. Shiozaki, T. Ishii, M. Kumagai, Top. Catal. 22 (2003) 205.
[28] M. Schuessler, M. Portscher, U. Limbeck, Catal. Today 79 (2003) 511.
[29] N. Iwasa, T. Mayanagi, W. Nomura, M. Arai, N. Takezawa, Appl. Catal. A Gen. 248 (2003) 153.
[30] J. Agrell, M. Boutonnet, J.L.G. Fierro, Appl. Catal. A Gen. 253 (2003) 213.
[31] X. Huang, L. Ma, M.S. Wainwright, Appl. Catal. A Gen. 257 (2004) 235.
[32] T. Shishido, Y. Yamamoto, H. Morioka, K. Takaki, K. Takehira, Appl. Catal. A Gen. 263 (2004) 249.
[33] C. Fukuhara, H. Ohkura, Y. Kamata, Y. Murakami, A. Igarashi, Appl. Catal. A Gen. 273 (2004) 125.
[34] V. Agarwal, S. Patel, K.K. Pant, Appl. Catal. A Gen. 279 (2005) 155.
[35] A. Karim, J. Bravo, A. Datye, Appl. Catal. A Gen. 282 (2005) 101.
[36] S. Liu, K. Takahashi, K. Uematsu, M. Ayabe, Appl. Catal. A Gen. 283 (2005) 125.
[37] P.H. Matter, U.S. Ozkan, J. Catal. 234 (2005) 463.
[38] J.B. Wang, C.-H. Li, T.-J. Huang, Catal. Lett. 103 (2005) 239.
[39] Y. Liu, T. Hayakawa, T. Tsunoda, K. Suzuki, S. Hamakawa, K. Murata, R. Shiozaki, T. Ishii, M. Kumagai, Top. Catal. 22 (2003) 205.
[40] W.-H. Cheng, I. Chen, J.-S. Liou, S.-S. Lin, Top. Catal. 22 (2003) 225.
[41] Y. Men, H. Gnaser, R. Zapf, V. Hessel, C. Ziegler, G. Kolb, Appl. Catal. A Gen. 277 (2004) 83.
[42] H. Oguchi, T. Nishiguchi, T. Matsumoto, H. Kanai, K. Utani, Y. Matsumura, S. Imamura, Appl. Catal. A Gen. 281 (2005) 69.
[43] A. Mastalir, B. Frank, A. Szizybalski, H. Soerijanto, A. Deshpande, M. Niederberger, R. Schomaecker, R. Schloegl, T. Ressler, J. Catal. 230 (2005) 464.
[44] G. Jacobs, B.H. Davis, Appl. Catal. A Gen. 285 (2005) 43.
[45] Y. Men, H. Gnaser, C. Ziegler, R. Zapf, V. Hessel, G. Kolb, Catal. Lett. 105 (2005) 35.
[46] S. Cavallaro, S. Freni, Int. J. Hydrogen Energy 21 (1996) 465.
[47] J. Llorca, N. Homs, J. Sales, P. Ramirez de la Piscina, J. Catal. 209 (2002) 306.
[48] J. Llorca, J.-A. Dalmon, P. Ramirez de la Piscina, N. Homs, Appl. Catal. A Gen. 243 (2003) 261.
[49] J. Llorca, P. Ramirez de la Piscina, J.-A. Dalmon, J. Sales, N. Homs, Appl. Catal. B Environ. 43 (2003) 355.
[50] J. Llorca, N. Homs, P. Ramirez de la Piscina, J. Catal. 227 (2004) 556.
[51] J.M. Guil, N. Homs, J. Llorca, P. Ramirez de la Piscina, J. Phys. Chem. B 109 (2005) 10813.
[52] J.P. Breen, R. Burch, H.M. Coleman, Appl. Catal. B Environ. 39 (2002) 65.
[53] F. Aupretre, C. Descorme, D. Duprez, Catal. Commun. 3 (2002) 263.
[54] E.C. Wanat, K. Venkataraman, L.D. Schmidt, Appl. Catal. A Gen. 276 (2004) 155.
[55] S. Duan, S. Senkan, Ind. Eng. Chem. Res. 44 (2005) 6381.
[56] J. Kugai, V. Subramani, C. Song, M.H. Engelhard, Y.-H. Chin, J. Catal. 238 (2006) 430.
[57] L.V. Mattos, F.B. Noronha, J. Catal. 233 (2005) 453.
[58] G.J. Hutchings, R.G. Copperthwaite, F.M. Gottschalk, R. Hunter, J. Mellor, S.W. Orchard, T. Sangiorgio, J. Catal. 137 (1992) 408.
[59] C. Rioche, S. Kulkarni, F.C. Meunier, J.P. Breen, R. Burch, Appl. Catal. B Environ. 61 (2005) 130.
[60] G. Jacobs, U.M. Graham, E. Chenu, P.M. Patterson, B.H. Davis, J. Catal. 229 (2005) 499.
[61] Y. Li, Q. Fu, M. Flytzani-Stephanopoulos, Appl. Catal. B 27 (2000) 179.
[62] T. Ressler, WinXAS 97 version 1.0, 1997.
[63] A. Laachir, V. Perrichon, A. Badri, J. Lamotte, E. Catherine, J.C. Lavalley, J. El Fallah, L. Hilaire, F. Le Normand, E. Quemere, G.N. Sauvion, O. Touret, J. Chem. Soc. Faraday Trans. 87 (1991) 1601.
[64] C. Li, K. Domen, K.-I. Maruya, T. Onishi, J. Catal. 125 (1990) 445.
[65] C. Binet, M. Daturi, J.C. Lavalley, Catal. Today 50 (1999) 207.
[66] A. Holmgren, B. Andersson, D. Duprez, Appl. Catal. B 22 (1999) 215.
[67] T. Shido, Y. Iwasawa, J. Catal. 141 (1993) 71.
[68] D. Duprez, Catal. Today 112 (2006) 17.
[69] D.C. Grenoble, M.M. Estadt, D.F. Ollis, J. Catal. 67 (1981) 90.
[70] G. Jacobs, S. Ricote, U.M. Graham, P.M. Patterson, B.H. Davis, Catal. Today 106 (2005) 259.
[71] M. Glinski, W. Szymanski, D. Lomot, Appl. Catal. A Gen. 281 (2005) 107.
[72] S. Freni, S. Cavallaro, N. Mondello, L. Spadaro, F. Frusteri, J. Power Sources 108 (2002) 53.
[73] G. Marino, F. Baronetti, M. Jobbagy, M. Laborde, Appl. Catal. A Gen. 238 (2003) 41–54.
[74] J. Comas, F. Marino, M. Laborde, N. Amadeo, Chem. Eng. J. 98 (2004) 61.
[75] J. Sun, X. Qiu, F. Wu, W. Zhu, W. Wang, S. Hao, Int. J. Hydrogen Energy 29 (2004) 1075.
[76] A.N. Fatsikostas, X.E. Verykios, J. Catal. 225 (2004) 439.
[77] F. Frusteri, S. Freni, V. Chiodo, L. Spadaro, O. Di Blasi, G. Bonura, S. Cavallaro, Appl. Catal. A Gen. 270 (2004) 1.
[78] J. Sun, X.-P. Qiu, F. Wu, W.-T. Zhu, Int. J. Hydrogen Energy 30 (2005) 437.
[79] K. Urasaki, K. Tokunaga, Y. Sekine, E. Kikuchi, M. Matsukata, Chem. Lett. 34 (2005) 668.
[80] F. Aupretre, C. Descorme, D. Duprez, D. Casanave, D. Uzio, J. Catal. 233 (2005) 464.